OXFORD

JNCI J Natl Cancer Inst (2015) 107(9): djv152

doi:10.1093/jnci/djv152
First published online June 10, 2015
Article

ARTICLE

Identification of a Novel Proto-oncogenic Network in Head and Neck Squamous Cell Carcinoma

Smitha R. Georgy, Michael Cangkrama, Seema Srivastava, Darren Partridge, Alana Auden, Sebastian Dworkin, Catriona A. McLean, Stephen M. Jane, Charbel Darido

Affiliations of authors: Department of Medicine, Monash University Central Clinical School, Prahran, Victoria 3004, Australia (SRG, MC, SS, DP, AA, SD, SMJ, CD); Department of Anatomical Pathology, Alfred Hospital, Prahran, Victoria 3004, Australia (CAM); Department of Hematology, Alfred Hospital, Prahran VIC 3181, Australia (SMJ).

Correspondence to: Stephen M. Jane, MBBS, PhD, Central Clinical School, Level 6, 99 Commercial Road, Melbourne, VIC 3004, Australia (e-mail: stephen.jane@monash.edu).

Abstract

Background: The developmental transcription factor *Grainyhead-like 3 (GRHL3)* plays a critical tumor suppressor role in the mammalian epidermis through direct regulation of PTEN and the PI3K/AKT/mTOR signaling pathway. *GRHL3* is highly expressed in all tissues derived from the surface ectoderm, including the oral cavity, raising a question about its potential role in suppression of head and neck squamous cell carcinoma (HNSCC).

Methods: We explored the tumor suppressor role of *Grhl3* in HNSCC using a conditional knockout (*Grhl3*$^{\Delta}$*/–/K14Cre+*) mouse line (n = 26) exposed to an oral chemical carcinogen. We defined the proto-oncogenic pathway activated in the HNSCC derived from these mice and assessed it in primary human HNSCC samples, normal oral epithelial cell lines carrying shRNA to *GRHL3*, and human HNSCC cell lines. Data were analyzed with two-sided chi square and Student's *t* tests.

Results: Deletion of *Grhl3* in oral epithelium in mice did not perturb PTEN/PI3K/AKT/mTOR signaling, but instead evoked loss of *GSK3B* expression, resulting in stabilization and accumulation of c-MYC and aggressive HNSCC. This molecular signature was also evident in a subset of primary human HNSCC and HNSCC cell lines. Loss of *Gsk3b* in mice, independent of *Grhl3*, predisposed to chemical-induced HNSCC. Restoration of GSK3B expression blocked proliferation of normal oral epithelial cell lines carrying shRNA to *GRHL3* (cell no., Day 8: Scramble ctl, $616 \pm 21.8 \times 10^3$ vs GRHL3-kd, $1194 \pm 44 \times 10^3$, $P < .001$; GRHL3-kd vs GRHL3-kd + GSK3B, $800 \pm 98.84 \times 10^3$, $P = .003$) and human HNSCC cells.

Conclusions: We defined a novel molecular signature in mammalian HNSCC, suggesting new treatment strategies targeting the GRHL3/GSK3B/c-MYC proto-oncogenic network.

Head and neck squamous cell carcinoma (HNSCC) is a heterogeneous disease, and different subclasses have been proposed based on etiology and mutational spectrum (1,2). Recently, analysis of whole exome sequencing from 74 HNSCC-normal pairs identified mutations in genes that regulate squamous differentiation (2), implicating dysregulation of this process as a driver of these cancers. On this basis, we hypothesized that the *Grainy head-like 3 (GRHL3)* gene, a member of a highly conserved family of transcription factors critical for epidermal development and homeostasis (3–5), may play a key role in prevention of HNSCC. Supporting this, the genomic region on chromosome 1p36.11 that contains the *GRHL3* gene is frequently deleted in human HNSCC (Supplementary Figure 1, available online). Mice lacking *Grhl3* throughout development exhibit a markedly thickened epidermis, perturbed expression of multiple epidermal differentiation markers and defective skin barrier formation, with newborn pups dying of dehydration (6,7). In adults, epidermal loss of *GRHL3* results in a proliferation/differentiation imbalance,

Received: July 14, 2014; **Revised:** January 9, 2015; **Accepted:** May 8, 2015

triggered by loss of expression of PTEN, a direct GRHL3 target, and activation of PI3K/AKT/mTOR signaling, which culminates in development of aggressive SCC. Reduced levels of GRHL3 and PTEN are also evident in human skin SCC, associated with increased expression of miR-21, which targets both tumor suppressors, thus defining the miR-21/GRHL3/PTEN-axis as a critical tumor suppressor pathway in this cancer (8). Increased levels of miR-21 are seen in some human HNSCCs and in HNSCC cell lines (8–10) associated with reduced levels of PTEN and GRHL3, suggesting that this axis is also critical for SCCs from these tissues. However, deletion of PTEN alone in oral epithelium in mice is not sufficient for promoting early or frequent HNSCC (11), in contrast to the highly penetrant skin tumors seen with epidermal deletion of PTEN (12). These findings raised the possibility of alternate GRHL3-dependent drivers of HNSCC, which we have explored in our *Grhl3* conditional knockout mouse model.

Methods

Experimental Animals

All experiments were pre-approved by the AMREP Animal Ethics Committee. The generation and genotyping of Grhl3$^{+/-}$ and *Grhl3*$^{\Delta/-}$*/K14Cre*$^{+}$ mice (referred to as conditional knockout [cKO] subsequently) have been described previously (8,13). GSK3B$^{+/-}$ mice (Sv/129) were purchased from The Jackson Laboratory (Stock No: 005817). Oral tumors were induced in three-month-old mice through the administration of 50 μg/mL 4-nitroquinolene-1 oxide (4-NQO) (Sigma-Aldrich) in drinking water for 16 weeks (cKO experiment) (14) or 100 μg/mL 4-NQO in drinking water for eight weeks (*Gsk3b*$^{+/-}$ experiment), followed by reversion to regular water and monitoring for 20 weeks (15). All animals underwent weekly oral cavity examination and were killed by cervical dislocation when distressed, or at week 20. A complete autopsy was performed on all animals and histopathological lesions in the tongue were scored by a certified pathologist.

Cell Culture, Expression of S9A GSK3B, and Knockdown of GRHL3

The human oral epithelial cell line (OKF-6) was purchased from Harvard Skin Disease Research Center. The human epidermal keratinocyte cell line (HaCaT) and the oral cancer cell lines SCC-25 (CRL-1628) and CAL-27 (CRL-2095) and the human embryonic kidney cell line (HEK293T) were purchased from ATCC. HNSCC cell lines (SCC-1, SCC-47, SCC-22B, SQ-20β), pharyngeal SCC cell line (Detroit 562), and hypopharyngeal SCC cell line (FaDu) were kindly provided by Dr. Cameron Johnstone (Peter MacCallum Cancer Centre, Melbourne, Australia) and validated phenotypically by gene expression analysis. HaCaT, HEK293T, SCC-1, SCC-47, SCC-22B, SQ-20b, Detroit 562, and FaDu cells were cultured in Dulbecco's modified Eagle's medium (DMEM) with 10% fetal bovine serum. OKF-6, SCC-25, and CAL-27 cells were cultured in Keratinocyte serum-free medium (K-SFM) with growth factors. All media were supplemented with 1% penicillin/streptomycin antibiotics and cultured in 5% CO_2 at 37°C.

The S9A GSK3B cDNA was obtained in the Addgene plasmid 14754 (16) and cloned into the doxycycline-inducible lentiviral vector pTRIPZ (Thermoscientific, MA) as an *XhoI*/*MluI* fragment. Lentivirus was generated in HEK293T cells through cotransfection of the psPAX2 and pMD2.G packaging plasmids and used to transinfect SCC cell lines. The cells were selected in puramycin (1 μg/mL) and treated with doxycycline (1 μg/mL) to induce protein expression. GIPZ Human GRHL3 shRNA (Clone ID: V2LHS_65975, Thermoscientific, MA) was used to knock down GRHL3 in OKF-6 and HaCaT cells, as described previously (8).

RNA Preparation, Quantitative Real-Time Polymerase Chain Reaction, Chromatin Immunoprecipitation, and Electrophoretic Mobility Shift Assays

Tongue epithelium from E18.5 Grhl3$^{+/+}$ and Grhl3$^{-/-}$ embryos and tumors from WT and cKO mice were homogenized in TRIzol (Invitrogen) and RNA extracted according to the manufacturer's instructions. For human samples, cancer cells were dissected out using LCM as described previously (8). Quantitative real-time polymerase chain reaction (qRT-PCR) was carried out as described previously, with Hypoxanthine-guanine phosphoribosyltransferase (HPRT) serving as the internal control in all experiments (13). A Student's *t* test was used to determine statistical differences in expression levels, with *P* values under .05 considered significant, and the results were analyzed using GraphPad Prism. The error bars in all expression analyses represent the standard deviation. Chromatin immunoprecipitation (ChIP) and electrophoretic mobility shift assays (EMSAs) were performed as described previously (8).

Immunoblot Analysis and Immunohistochemistry

Tongue epithelium from E18.5 wild-type and Grhl3$^{-/-}$ embryos, tongue tumors from wild-type, and cKO mice were lysed in RIPA buffer containing protease inhibitors. Insoluble materials were removed by centrifugation. Immunoblots were then performed as described previously (8). Densitometry on immunoblots was performed using Photoshop software and values normalized to respective loading controls. The relative expression levels were calculated in comparison with WT controls. For immunohistochemistry (IHC), tissues were collected and fixed in 4% paraformaldehyde (PFA) overnight, and analyzed as described previously (8). Antibodies used for immunoblotting and IHC and the dilutions employed are shown in Supplementary Table 1 (available online). For IHC, staining intensity was quantified using Photoshop software, and a Student's *t* test was used to assess the significance of differences between samples.

Statistical Analyses

The differences in tumor-free survival were analyzed using a two-sided chi square test. A two-sided Student's *t* test was used to determine statistical differences in gene expression levels using qRT-PCR. In proliferation assays, the differences in cell number were analyzed using two-sided Student's *t* test. All statistical analyses were performed using GraphPad scientific software (version 6.e, GraphPad software, Inc). The error bars in all analyses represent the standard deviation.

Results

Effects of *Grhl3* Deletion During Embryogenesis on Oral Epithelium

Our initial experiments examined the degree of proliferation of tongue epithelium in the constitutive *Grhl3*-null mice. Histologically, this epithelium was markedly thickened at embryonic day (E) 18.5 in the *Grhl3*$^{-/-}$ animals compared with wild-type (*Grhl3*$^{+/+}$) controls (Figure 1, A and B), and expression

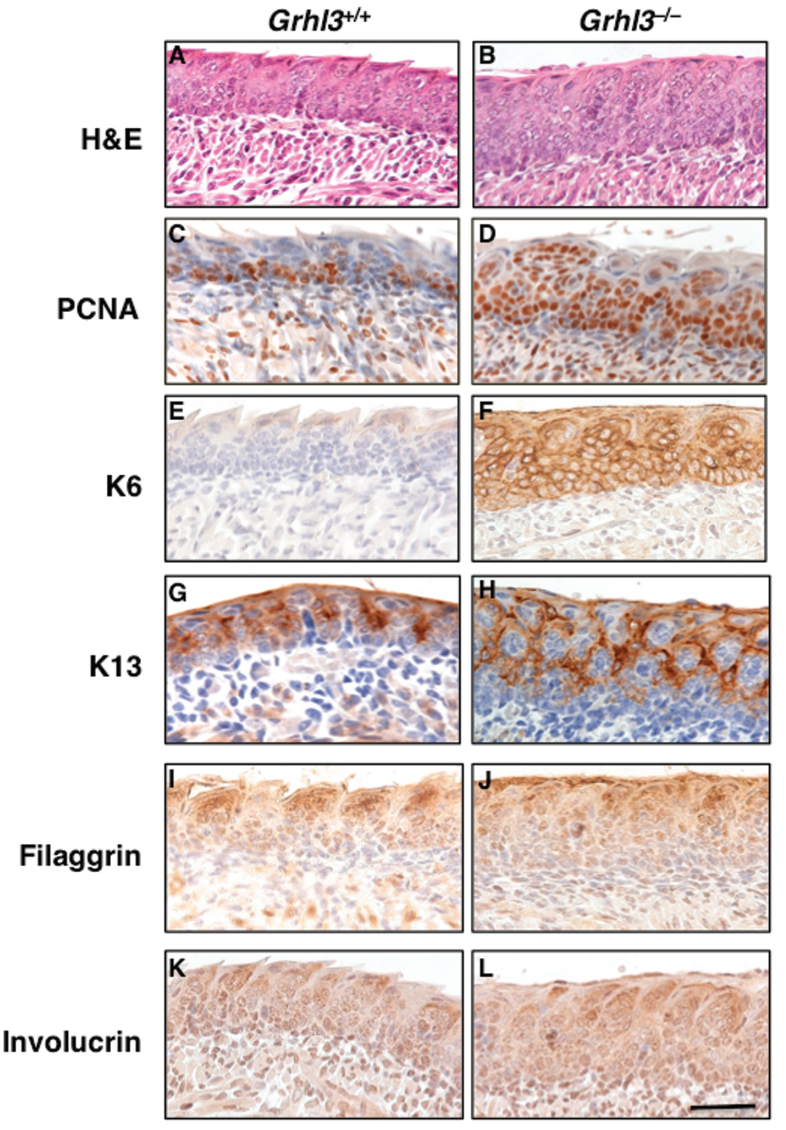

Figure 1. Hyperproliferation of tongue epithelium in *Grhl3*$^{-/-}$ mice. **A and B)** Hematoxylin and eosin. **C and D)** Proliferating cell nuclear antigen. **E and F)** K6. **G and H)** K13. **I and J)** Filaggrin. **K and L)** Involucrin immunohistochemistry staining of tongue epithelium from E18.5 *Grhl3*+/+ and *Grhl3*–/– embryos. **Scale bar** corresponds to 50 μm. H&E = hematoxylin and eosin; PCNA = proliferating cell nuclear antigen.

of the proliferative marker PCNA was expanded (Figure 1, C and D). Expression of keratin (K) 6, another marker of hyperproliferation, was also increased in the tongue epithelium of *Grhl3*$^{-/-}$ embryos (Figure 1, E and F) (17,18), whereas the differentiation markers K13, filaggrin, and involucrin were unaltered between *Grhl3*$^{-/-}$ and *Grhl3*$^{+/+}$ embryos (Figure 1, G-L).

Analysis of *Grhl3* Deletion in Oral Epithelium for Susceptibility to Spontaneous and Chemical-Induced HNSCC

As constitutive deletion of *Grhl3* during development leads to neonatal lethality, we have previously generated a *Grhl3* conditional knockout line to allow functional studies in adult mice (8). The *K14Cre* transgene used in this line induces minimal deletion in embryogenesis but achieves high levels of deletion in all tissues derived from the surface ectoderm in adulthood. Analysis of genomic DNA derived from tongue epithelium from these mice revealed a 1:1 ratio of undeleted (*flox*) to deleted (Δ) *Grhl3* alleles at four weeks of age, which had reached almost 100% deletion by 12 weeks. (Figure 2A), and this efficiency was reflected in expression levels, with a nine-fold decrease ($P = .002$) in *Grhl3* expression in the cKO mice (Figure 2B). Aging cKO mice developed spontaneous tumors in the tongue and oral mucosa, with 80% affected by one year (Supplementary Figure 2, A-C, available online). Exposure of cohorts of cKO mice (n = 26) and wild-type controls (n = 30) to the oral chemical carcinogen 4-NQO (14) accelerated tumor development. At 20 weeks, 85% of the cKO mice had developed tumors that necessitated death, compared with 35% of the WT controls (Figure 2C). At autopsy, histologically confirmed highly invasive SCC were identified in the tongue and floor of the mouth (Figure 2D; Supplementary Figure 2D, available online), larynx (Supplementary Figure 2E, available online), and pharynx (Supplementary Figure 2F, available online) in 39% of cKO mice, and papillomas in an additional 45%, whereas control animals displayed SCC in only 3% of cases, with papillomas (30%) or dysplasia (27%) being far more prevalent (Figure 2E). Expression of *Grhl3* was absent in tumors from cKO mice (Figure 2F), and, commensurate with this, genomic DNA derived from tumors revealed complete deletion

ARTICLE

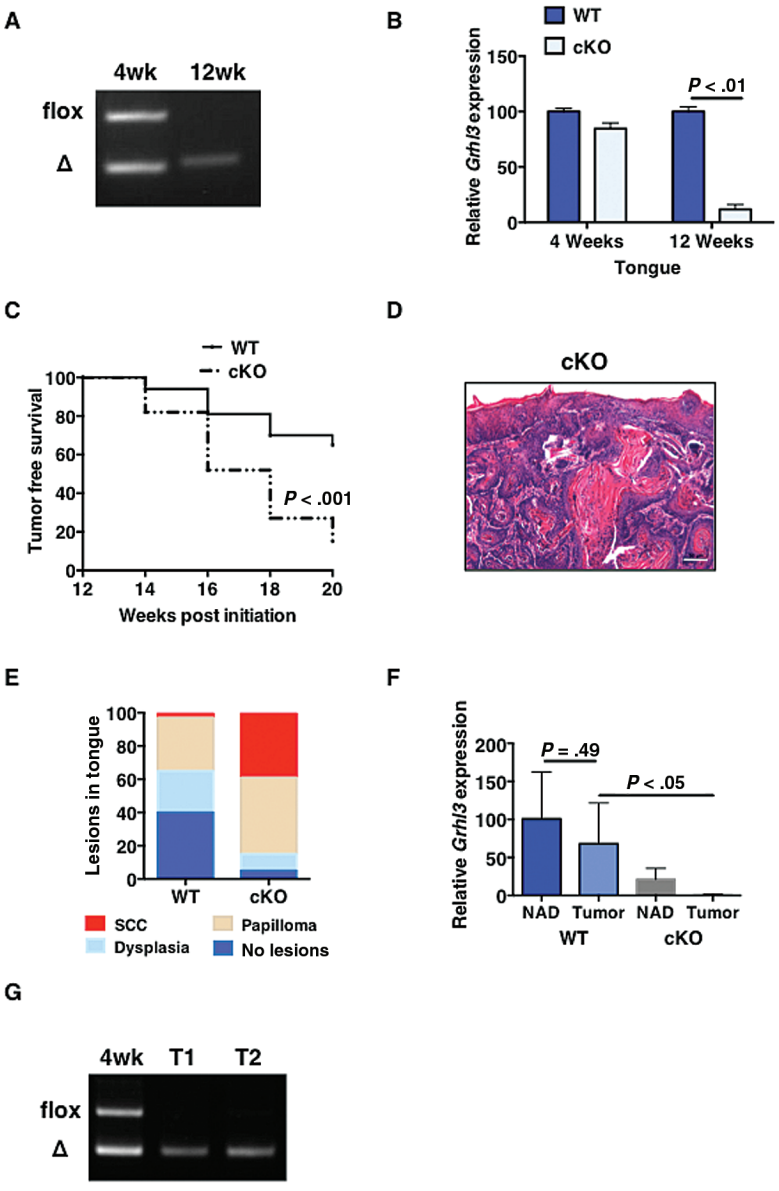

Figure 2. *Grhl3* as a tumor suppressor in head and neck squamous cell carcinoma (HNSCC). **A)** Polymerase chain reaction (PCR) analysis of deletion in genomic DNA from tongue epithelium of four-week-old and 12-week-old conditional knockout (cKO) mice. The undeleted (flox) band of 425 bp, and the deleted (Δ) band of 282 bp are indicated. **B)** Quantitative real-time polymerase chain reaction (qRT-PCR) of *Grhl3* expression in tongue epithelium from wild-type (WT) and cKO mice at four and 12 weeks. HPRT served as internal control. Mean of three independent experiments with each genotype at each time-point ± standard deviation. At 12 weeks, a nine-fold decrease in Grhl3 expression in cKO mice ($P = .002$, two-sided Student's *t* test) was observed. **C)** Oral tumor–free survival in 4-NQO–treated WT (n = 30) and cKO mice (n = 26). The differences in tumor-free survival were statistically significant using a two-sided chi square test ($P < .001$). **D)** Hematoxylin and eosin (H&E) staining of HNSCC arising in cKO mice. **Scale bar** corresponds to 50 μm. **E)** Scoring of tongue lesions in 4-NQO–treated WT (n = 30) and cKO mice (n = 26) based on histopathology. **F)** qRT-PCR of *Grhl3* expression in tumors arising from 4-NQO–treated WT (n = 7) and cKO mice (n = 20). The differences in expression between WT and cKO-derived tissues were statistically significant ($P = .02$) using a two-sided Student's *t* test. Mean of three independent experiments ± SD. **G)** Genomic PCR showing *Grhl3* deletion in tongue tumor samples compared with the tongue of four-week-old cKO mice. cKO = conditional knockout; SCC = squamous cell carcinoma; WT = wild-type.

(Figure 2G). In contrast, *Grhl3* expression was conserved in tumors derived from wild-type mice (Figure 2F).

In the epidermis, deletion of *Grhl3* induces loss of expression of PTEN, activation of PI3K/AKT/mTOR signalling, and a complete absence of p-ERK1/2 expression, culminating in SCC (8). To ascertain whether the same proto-oncogenic network was operational in *Grhl3*-deficient oral epithelium and HNSCC, we initially analyzed the oral epithelium from young (12-week-old) cKO mice and WT controls. Surprisingly, PTEN protein levels were not reduced and expression of p-ERK1/2 was maintained (Figure 3A). In keeping with this, p-AKT levels were not increased in the *Grhl3*-deficient epithelium (Figure 3B; Supplementary Figure 3A, available online). Similar results were also obtained in HNSCC from these mice, with *Pten* mRNA (Figure 3C) and protein levels (Figure 3D; Supplementary Figure 3B, available online) comparable with those seen in tumors from WT mice, with reduced levels of p-AKT (Figure 3E; Supplementary Figure 3C, available online) and persistent expression of p-ERK1/2 (Figure 3D; Supplementary Figure 3B, available online). These findings suggest that a different signaling pathway downstream of *Grhl3* serves as the driver of HNSCC in this model.

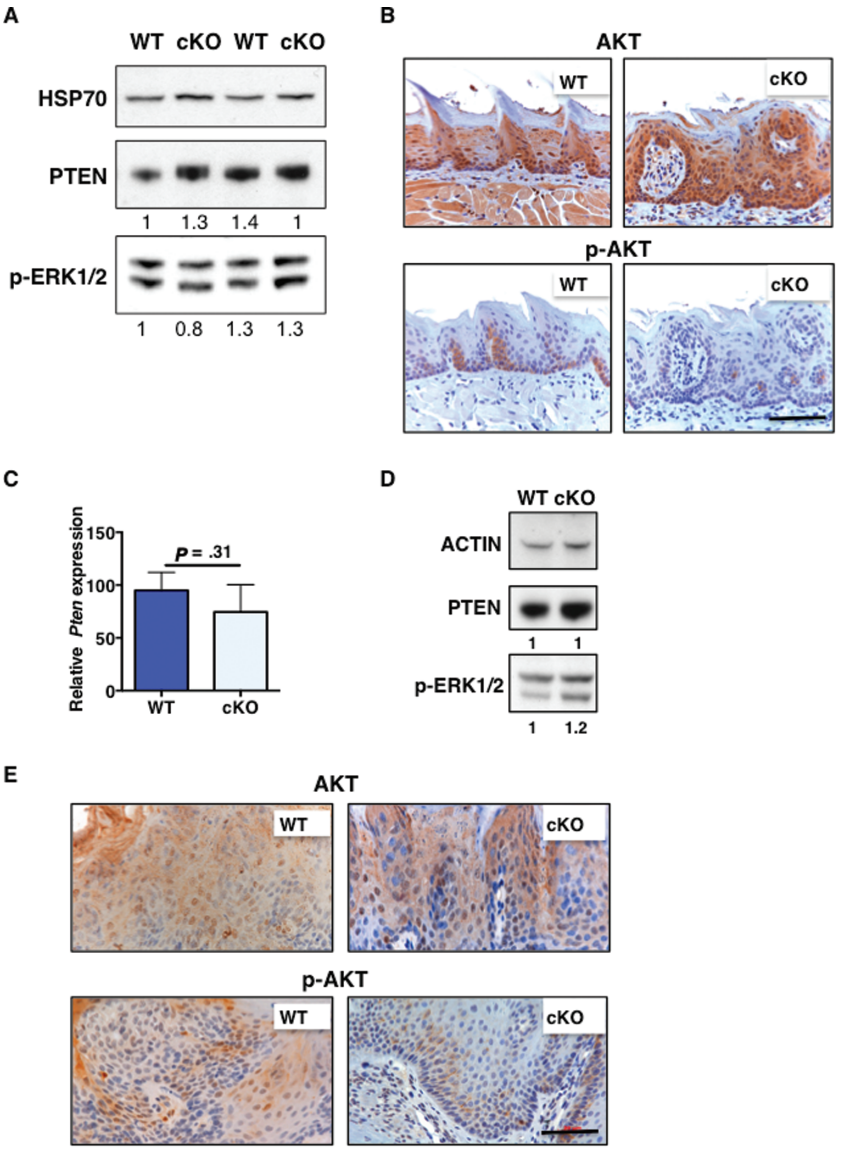

Figure 3. Analysis of PI3K/AKT signalling in head and neck squamous cell carcinoma (HNSCC) from *Grhl3*-deficient mice. **A)** Immunoblots of PTEN and p-ERK1/2 expression in tongue epithelium from 12-week-old wild-type (WT) and conditional knockout (cKO) mice. HSP70 served as the loading control. Quantitation of expression relative to the WT control and normalized to the loading control as measured by densitometry is shown under each lane. **B)** Immunohistochemistry (IHC) analysis of tongue epithelium from 12-week-old WT and cKO mice using AKT and p-AKT antibodies. **Scale bar** corresponds to 50 μm. The staining intensity of p-AKT was statistically significant between genotypes (two-sided Student's *t* test $P < .001$). **C)** Quantitative real-time polymerase chain reaction (qRT-PCR) of Pten expression in tumors arising from 4-NQO–treated WT and cKO mice. The differences in expression between WT and cKO-derived tissues were not statistically significant ($P = .31$) using a two-sided Student's *t* test. Mean of three independent experiments ± SD. **D)** Immunoblot of PTEN and p-ERK1/2 in tumors arising from 4-NQO–treated WT and cKO mice. Actin served as the loading control. Quantitation of expression relative to the WT control and normalized to the loading control as measured by densitometry is shown under each lane. **E)** IHC analysis of tongue tumors from WT and cKO mice using AKT and p-AKT antibodies. **Scale bar** corresponds to 50 μm. The staining intensity of p-AKT was statistically significant between genotypes (two-sided Student's *t* test $P = .0057$). cKO = conditional knockout; WT = wild-type.

GSK3B as a Direct Transcriptional Target Gene of GRHL3

The DNA consensus-binding site for the human and *Drosophila* GRHL factors (AACCGGTT) has been conserved across 700 million years (6). Based on this, we have successfully used a phylogenetic approach to identify GRHL3 binding motifs in regulatory sequences conserved across all placental mammals (8,19). Re-interrogation of this dataset identified a highly conserved GRHL site in the promoter of the *GSK3B* gene (Figure 4A) that encodes a multifunctional serine/threonine kinase involved in epithelial cell homeostasis and transformation (20). A tumor suppressor role for *GSK3B* in oral cancer has been postulated, although not demonstrated experimentally (21). Specific binding of GRHL3 to the *GSK3B* site was demonstrated in vitro in EMSA (Supplementary Figure 4, available online), and in vivo by chromatin immunoprecipitation in the human normal oral epithelial cell line OKF-6 (Figure 4B). Expression of *Gsk3b* was reduced in tongue epithelium derived from E18.5 *Grhl3* null embryos (two-fold difference, $P = .002$ for Figure 4C) (Figure 4, C and D) and cKO mice (two-fold difference, $P = .006$ for Figure 4E) (Figure 4, E and F).

A 2.0- to 3.3-fold reduction in GSK3B expression was also observed in laser capture microdissected (LCM) HNSCC and adjacent normal epithelium from 4-NQO–treated cKO mice compared with controls ($P = .006$) (Figure 5, A and B; Supplementary

ARTICLE

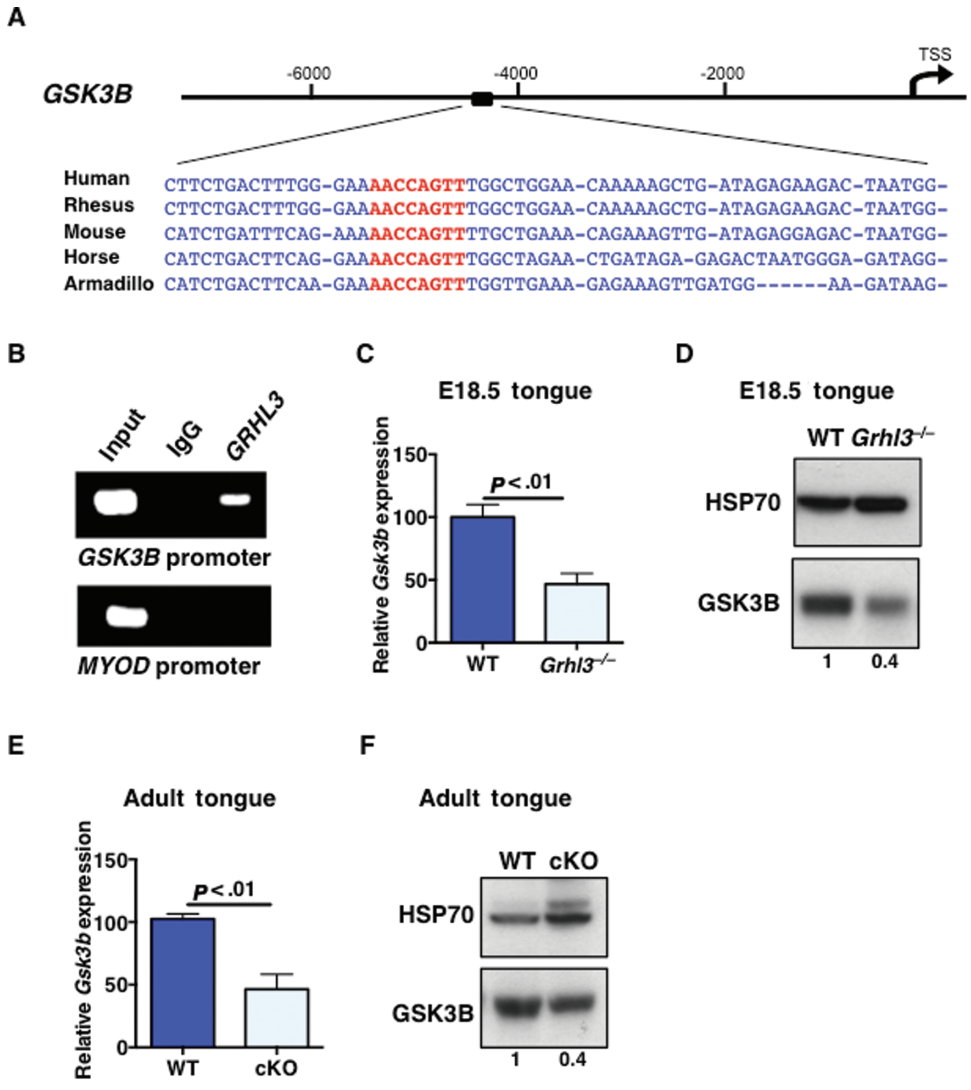

Figure 4. *Gsk3b* as a direct transcriptional target of GRHL3. **A)** Alignment of the promoter regions of *GSK3B* genes from the indicated species. The GRHL3 DNA binding consensus sequence is shown in **red**. **B)** Chromatin immunoprecipitation analysis of endogenous GRHL3 on the *GSK3B* promoter. Chromatin from the human oral epithelial cell line OKF-6 was immunoprecipitated using antisera to GRHL3 and amplified with *GSK3B* primers. Preimmune sera (IgG) and the muscle-specific *MYOD* promoter were used as negative controls, and the input chromatin is shown. **C)** Quantitative real-time polymerase chain reaction (qRT-PCR) and **(D)** immunoblot of *GSK3B* expression in tongue epithelium from E18.5 wild-type (WT) and *Grhl3*–/– E18.5 embryos. For **(C)**, the differences in expression between WT and conditional knockout (cKO)–derived tissues were statistically significant ($P = .002$) using a two-sided Student's *t* test. Mean of three independent experiments ± SD. For **(D)**, HSP70 served as the loading control. Quantitation of expression relative to the WT control and normalized to the loading control as measured by densitometry is shown under each lane. **E)** qRT-PCR and **(F)** immunoblot of GSK3B expression in tongue epithelium from WT and cKO adult mice. For **(E)**, the differences in expression between WT and cKO-derived tissues were statistically significant ($P = .006$) using a two-sided Student's *t* test. Mean of three independent experiments ± SD. For **(F)**, HSP70 served as the loading control. Quantitation of expression relative to the WT control and normalized to the loading control as measured by densitometry is shown under each lane. cKO = conditional knockout; WT = wild-type.

Figure 5A, available online). IHC on sections from papillomas and HNSCC from cKO mice compared with papillomas from WT controls also showed reduced GSK3B expression (Figure 5C; Supplementary Figure 5B, available online). To determine whether loss of GSK3B expression in the setting of wild-type levels of GRHL3 also enhanced HNSCC formation, we obtained mice heterozygous for a targeted deletion of the *Gsk3b* allele (*Gsk3b*$^{+/-}$) and confirmed reduced levels of *Gsk3b* mRNA in the tongue epithelium by two-fold ($P = .04$) (Figure 5D). This was accompanied by hyperproliferation of the oral epithelium, with thickening and increased Ki-67 staining compared with WT controls (Supplementary Figure 6, A and B, available online). We exposed these mice, and WT controls to 4-NQO (n = 7 in each group) (Figure 5E), and demonstrated that 85% of the *Gsk3b*$^{+/-}$ cohort exhibited either papillomas or frank SCC by 20 weeks, comparable with the cKO mice. No WT animals developed HNSCC. Expression of *Gsk3b* was reduced in the HNSCC and papillomas from the *Gsk3b*$^{+/-}$ mice almost two-fold ($P = .02$), but not the papillomas from the controls (Figure 5F). Expression of *Grhl3* was not statistically significantly different in tumors from both groups (Figure 5G). Taken together, these data suggest that GSK3B is the critical downstream target of GRHL3 for prevention of HNSCC.

Analysis of Signaling Pathways Induced by Loss of GSK3B

One of the known GSK3B substrates implicated in HNSCC pathogenesis is the proto-oncogene c-MYC, which is targeted for

ARTICLE

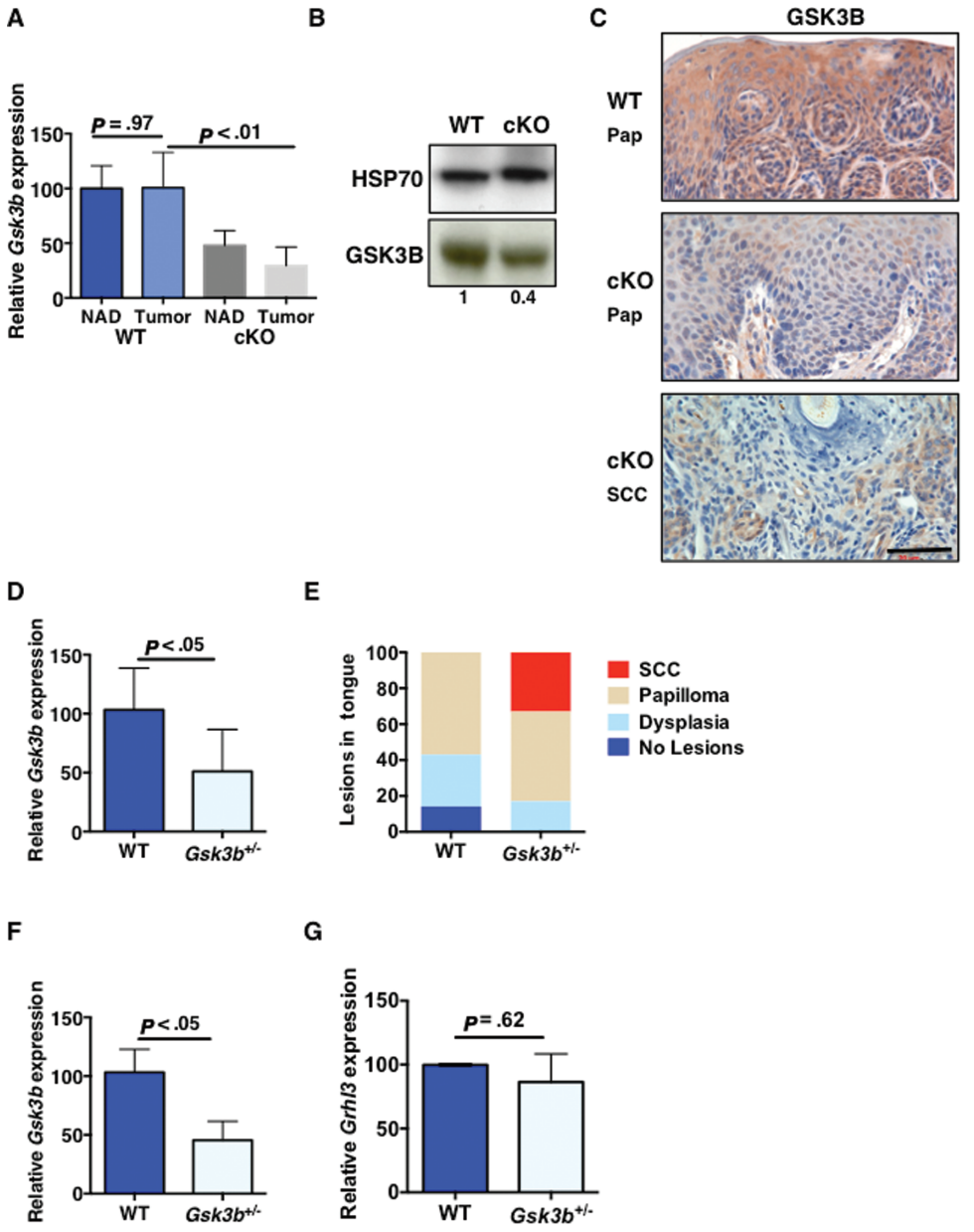

Figure 5. GSK3B as a tumor suppressor gene in head and neck squamous cell carcinoma (HNSCC). **A)** Quantitative real-time polymerase chain reaction (qRT-PCR) of *Gsk3b* expression in tumors and adjacent normal tissue (NAD) from 4-NQO–treated wild-type (WT) and conditional knockout (cKO) mice. The differences in expression between WT and cKO-derived tissues were statistically significant ($P = .006$) using a two-sided Student's *t* test. Mean of four independent experiments ± SD. **B)** Immunoblot of GSK3B expression in tumors arising from 4-NQO–treated WT and cKO mice. HSP70 served as the loading control. Quantitation of expression relative to the WT control and normalized to the loading control as measured by densitometry is shown under each lane. **C)** Immunohistochemistry (IHC) analysis of tongue tumors from WT and cKO mice using GSK3B antibody. **Scale bar** corresponds to 50 μm. The staining intensity of GSK3B was statistically significant between genotypes (two-sided Student's *t* test $P = .0012$). **D)** Relative *Gsk3b* expression in tongue epithelium by qRT-PCR in WT and *Gsk3b*+/– mice. The differences in expression between WT and *Gsk3b*+/–-derived tissues were statistically significant ($P = .04$) using a two-sided Student's *t* test. Mean of three independent experiments ± SD. **E)** Scoring of tongue lesions in 4-NQO–treated WT (n = 7) and *Gsk3b*+/– mice (n = 6) based on histopathology. **F)** qRT-PCR of *Gsk3b* expression in tumors arising from 4-NQO–treated WT and *Gsk3b*+/– mice. The differences in expression between WT and *Gsk3b*+/–-derived tissues were statistically significant ($P = .02$) using a two-sided Student's *t* test. Mean of three independent experiments ± SD. **G)** qRT-PCR of *Grhl3* expression in tumors arising from 4-NQO–treated WT and *Gsk3b*+/– mice. The differences in expression between WT and *Gsk3b*+/– tissues were not statistically significant ($P = .62$) using a two-sided Student's *t* test. Mean of three independent experiments ± SD. cKO = conditional knockout; SCC = squamous cell carcinoma; WT = wild-type.

ubiquitination and proteosomal degradation by GSK3B-dependent phosphorylation of threonine (T) 58 (22–24). Consistent with this, the reduced GSK3B levels observed in tongue epithelium were associated with increased expression of c-MYC protein in both E18.5 *Grhl3*$^{-/-}$ embryos (Figure 6A) and cKO mice (Figure 6B). HNSCC derived from cKO mice also exhibited increased expression of c-MYC protein (Figure 6C; Supplementary Figure 7A, available online) but no increase in *c-Myc* mRNA levels (Figure 6D), indicating that a post-translational, and not a transcriptional, mechanism was driving the enhanced expression. IHC on sections from HNSCC and papillomas from cKO mice confirmed increased levels of c-MYC, with almost complete absence of phosphorylated T58 c-MYC (Figure 6E; Supplementary Figure 7B, available online). This was also observed in spontaneous tumors from

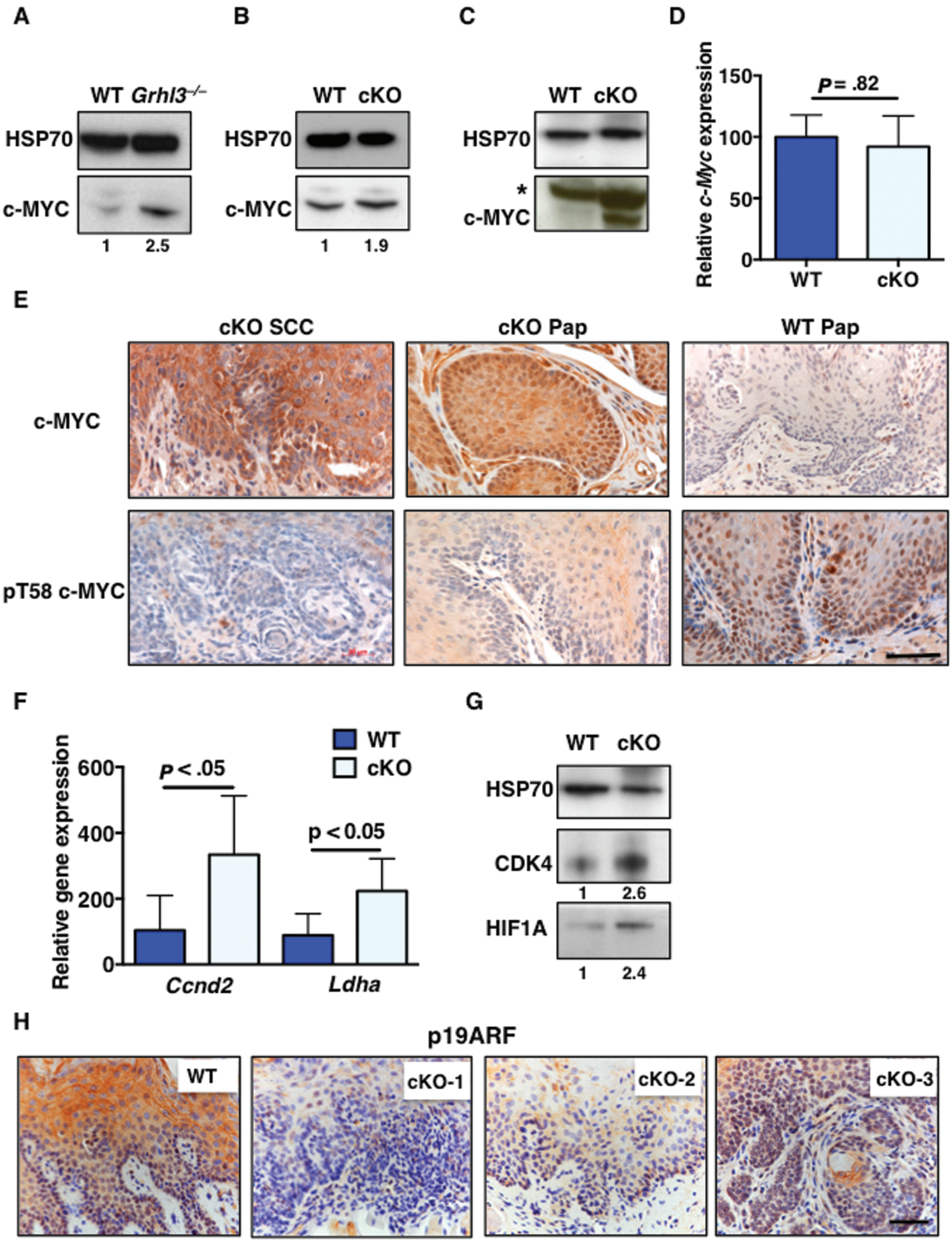

Figure 6. Transcriptional loss of *Gsk3b* and stabilization of c-MYC. Immunoblot of c-MYC expression in tongue epithelium from **(A)** wild-type (WT) and *Grhl3–/–* E18.5 embryos. **B)** WT and conditional knockout (cKO) adult mice. HSP70 served as the loading control. Quantitation of expression relative to the WT control and normalized to the loading control as measured by densitometry is shown under each lane. **C)** Immunoblot of c-MYC in tumors arising from tongue in 4-NQO–treated WT and cKO mice. Actin served as the loading control. The **asterisk** in the *Myc* panel denotes a nonspecific band. **D)** Quantitative real-time polymerase chain reaction (qRT-PCR) of *c-Myc* expression in tumors arising from tongue in 4-NQO–treated WT and cKO mice. The differences in expression between WT and cKO-derived tissues were not statistically significant ($P = .82$) using a two-sided Student's *t* test. Mean of four independent experiments ± SD. **E)** Immunohistochemistry (IHC) analysis of tongue tumors from cKO and WT mice using c-MYC and pT58 c-MYC antibodies. **Scale bar** corresponds to 50 μm. The staining intensity of c-MYC ($P = .048$) and pT58 c-MYC ($P < .001$) was statistically significant between genotypes using a two-sided Student's *t* test. **F)** qRT-PCR of *Ccnd2* and *Ldha* expression in tumors arising from 4-NQO–treated WT and cKO mice. The differences in expression between WT and cKO-derived tissues were statistically significant ($P = .04$) using a two-sided Student's *t* test. Mean of four independent experiments ± SD. **G)** Immunoblot of CDK4 and HIF1A in tumors arising from 4-NQO–treated WT and cKO mice. HSP70 served as the loading control. Quantitation of expression relative to the WT control and normalized to the loading control as measured by densitometry is shown under each lane. **H)** IHC analysis of tongue tumors from WT and cKO mice using p19ARF antibodies. **Scale bar** corresponds to 50 μm. The staining intensity of p19ARF ($P < .001$) was statistically significant between genotypes using a two-sided Student's *t* test. cKO = conditional knockout; SCC = squamous cell carcinoma; WT = wild-type.

cKO mice (not shown), indicating that these effects occur independently of the carcinogenesis protocol. Tumors from WT mice exhibited reduced expression of c-MYC associated with elevated levels of pT58 c-MYC (Figure 6E; Supplementary Figure 7B, available online), whereas tumors derived from *Gsk3b*$^{+/-}$ mice immunophenocopied cKO tumors with increased levels of c-MYC (Supplementary Figure 7C, available online). Downstream targets of c-MYC involved in cell cycle progression (cyclin D2, CDK4), cellular metabolism (LDHA), and angiogenesis (HIF1A) were also elevated more than two-fold ($P = .04$) in the HNSCC from cKO compared with WT mice (Figure 6, F and G), confirming the functional activity of elevated proto-oncogene.

Low levels of deregulated MYC are competent to drive cellular proliferation and oncogenesis, but higher levels of overexpression are associated with elevated levels of pARF and apoptosis (25). IHC on HNSCC from cKO (Figure 6H) and *Gsk3b*$^{+/-}$ (Supplementary Figure 7D, available online) mice demonstrated minimal p19ARF expression compared with an HNSCC from a WT animal, which served as the control.

Analysis of the GRHL3/GSK3B/c-MYC Proto-oncogenic Axis in Human HNSCC

GRHL3 levels are reduced in almost all human HNSCC compared with adjacent normal tissues (8). In a subset of these cancers, levels of PTEN are also reduced (8), consistent with published data (2,26). To further explore the relationship between *GRHL3*, *GSK3B*, and *PTEN* in human HNSCC, we performed qRT-PCR for the three factors on LCM-derived tumor tissue and adjacent normal epithelium from 24 consecutive operative specimens (Figure 7A). All the tumors exhibited reduced *GRHL3* levels (below 50% of adjacent normal tissue, although in most expression was undetectable), emphasizing the importance of this transcription factor as a driver of HNSCC. Three distinct subsets of equivalent number were identified based on *GSK3B* and *PTEN* expression (Figure 7A): low *GSK3B*, high *PTEN* (samples 1–7); low *GSK3B*, low *PTEN* (samples 8–16); and normal *GSK3B*, low *PTEN* (samples 17–23). No association between the tissue of origin of the SCC and *GSK3B* or *PTEN* levels was observed. Loss of pT58 c-MYC was only observed in samples 1 to 16, in which GSK3B levels were low, irrespective of the levels of PTEN expression (Figure 7B).

To evaluate the loss of *GSK3B* as a driver of cellular proliferation in normal oral epithelium and HNSCC, we initially generated a human oral epithelial cell line (OKF-6) in which the expression of GRHL3 had been knocked down using a specific shRNA-containing lentivirus (GRHL3-kd) (Figure 7C) (19). A line transduced with a scrambled control (Scr) shRNA served as the control. The level of GSK3B was reduced in the GRHL3-kd line compared with control, and the level of c-MYC was increased, with a concomitant reduction observed in p-c-MYC. The GRHL3-kd cells proliferated more rapidly than the Scr cells (cell number: $616 \pm 21.8 \times 10^3$ vs $1194 \pm 44 \times 10^3$ at day 8, $P < .001$) (Figure 7D). Transduction of the GRHL3-kd cells with an expression vector carrying a mutant form of GSK3B containing an alanine substitution for serine 9 (S9A GSK3B), which prevents phosphorylation and enzymatic inactivation (16), resulted in increased levels of total GSK3B (wild-type and mutant forms). Increased levels of phosphorylated S9 GSK3B (pS9 GSK3B) were not observed because of the mutation of the S9 residue, indicating that the increased expression of GSK3B was in the active form. Consistent with the elevated levels of active GSK3B, c-MYC expression was reduced and p-c-MYC expression increased. As a consequence, the growth of the GRHL3-kd cells expressing S9A GSK3B was slowed (cell number: $800 \pm 98.84 \times 10^3$ at day 8, ($P = .003$) when compared with GRHL3-kd cells (Figure 7D).

To test this in the context of HNSCC, we initially examined two human HNSCC cell lines (CAL-27 and SCC-25) that exhibit reduced expression of *GRHL3* and *GSK3B* compared with their normal counterpart, OKF-6 (Figure 8A). We transduced these cells with a doxycycline-inducible S9A GSK3B containing vector and quantitated GSK3B, c-MYC, and p-c-MYC expression and growth kinetics in uninduced and induced cells (Figure 8, B-E). In both lines, increased expression of the active form of GSK3B in induced cells resulted in reduced levels of c-MYC, increased p-c-MYC, and reduced cellular proliferation to rates comparable with the nonmalignant OKF-6 line. On day 8, SCC-25 cell numbers were reduced from $754 \pm 75 \times 10^3$ to $389 \pm 75.99 \times 10^3$, with overexpression of GSK3B ($P < .001$) (Figure 8E), and CAL-27 cell numbers were reduced from $1011 \pm 74.9 \times 10^3$ to $640 \pm 132.9 \times 10^3$, with overexpression of GSK3B ($P = .04$) (Figure 8C)—both comparable with the numbers of OKF-6 cells ($512 \pm 33.9 \times 10^3$). Doxycycline alone had no effect on the growth kinetics of untransfected cells (data not shown). Similar effects on growth kinetics were observed with S9A GSK3B transduction in multiple other human HNSCC lines that exhibited low levels of GRHL3 and GSK3B expression compared with OKF-6 cells (Supplementary Figure 8, A-D, available online). These findings support our hypothesis that loss of GRHL3/GSK3B expression is a key molecular driver of a subset of human HNSCC.

Assessing the Mechanism Underpinning Differential Proto-oncogenic Activation in HNSCC vs Skin SCC

To compare the proto-oncogenic axes induced by loss of *Grhl3* in oral epithelium vs skin, we examined whether activation of the GSK3B/c-MYC network occurred in GRHL3-deficient adult epidermis. Immunoblots on skin from 12-week-old cKO mice and WT littermate controls displayed no loss of GSK3B expression or increase in c-MYC levels (Supplementary Figure 9A, available online). In normal epidermis and SCC derived from cKO mice, in which *Grhl3* levels are undetectable (8), no loss of GSK3B or pT58 c-MYC was observed (Supplementary Figure 9, B and C, available online). Similar findings were evident in primary skin SCC from humans (Supplementary Figure 9, B and C, available online). To explore this apparent paradox, we transfected a normal human keratinocyte cell line (HaCaT) with the shRNA to GRHL3, achieving an 80% knockdown of expression compared with a scrambled shRNA control. We then measured the levels of PTEN and GSK3B in these cells and compared them to the levels observed in OKF-6 *Grhl3*-kd cells (Supplementary Figure 9D, available online). In the keratinocytes, loss of GRHL3 was associated with a eight-fold reduction in PTEN ($P < .001$) but no loss of GSK3B expression ($P = .20$), consistent with our data in the GRHL3-deficient skin and SCC from human and mouse. In contrast, PTEN expression was preserved in the OKF-6 *Grhl3*-kd cells ($P = .25$), but GSK3B levels were reduced two-fold ($P = .034$), as shown previously. These findings suggest that the different proto-oncogenic axes in HNSCC (GRHL3/GSK3B/c-MYC) vs skin SCC (GRHL3/PI3K/AKT/mTOR) are partly established in response to target gene specificity of GRHL3 in the different tissues of origin.

Discussion

We have identified a novel proto-oncogenic pathway in a subset of mammalian HNSCCs that offers potential insights for treatment selectivity. Using mouse models, primary human samples,

ARTICLE

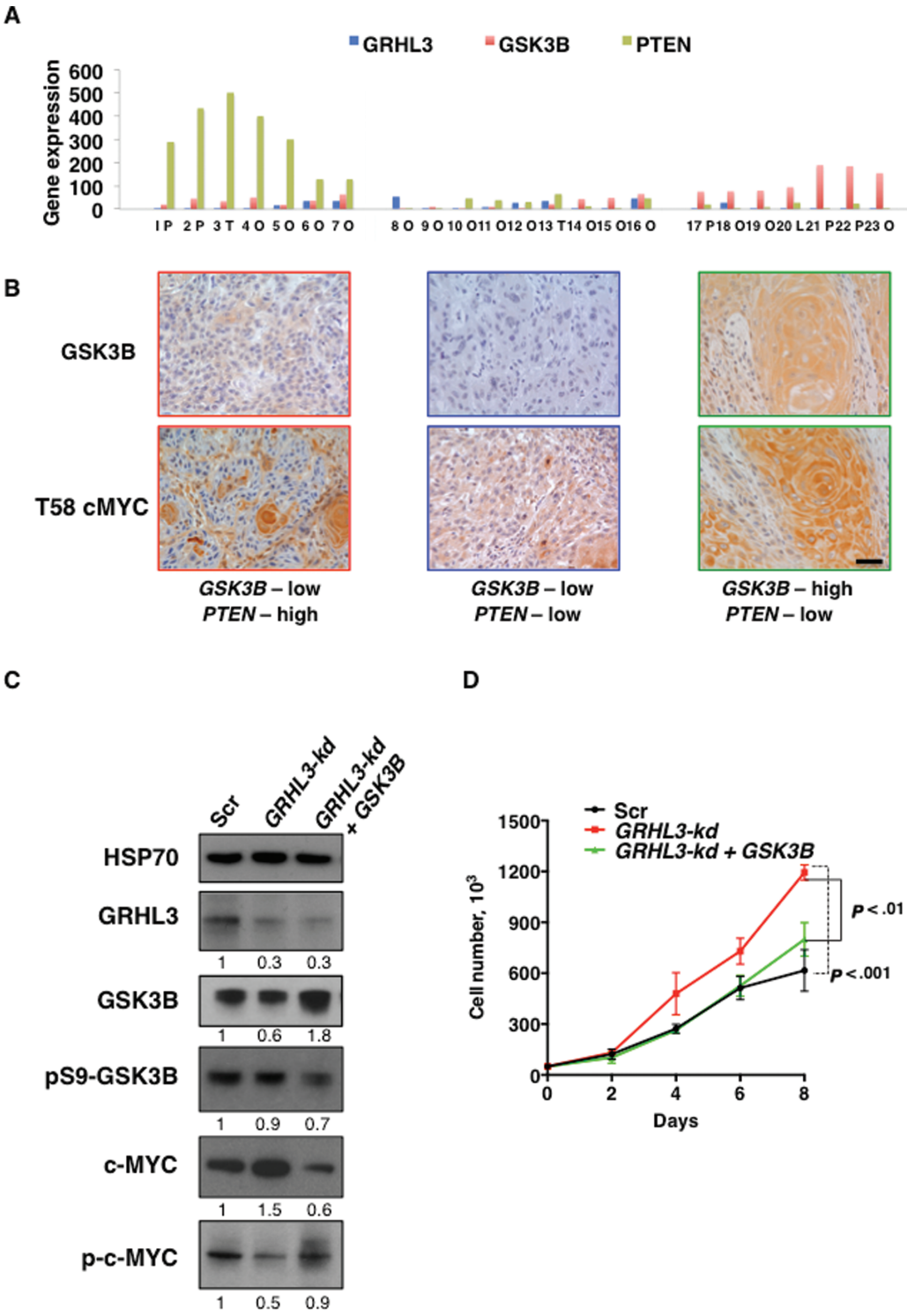

Figure 7. Analysis of the GRHL3/GSK3B/c-MYC proto-oncogenic axis in a subset of human head and neck squamous cell carcinoma (HNSCC). **A)** Quantitative real-time polymerase chain reaction (qRT-PCR) of *GRHL3*, *GSK3B*, and *PTEN* expression in 24 human HNSCC samples compared with adjacent non–tumor containing tissue. HPRT served as the control. L = larynx; O = oral cavity; P = pharynx; T = tongue. **B)** Immunohistochemistry (IHC) analysis of representative human HNSCC with different molecular signatures using GSK3B and pT58 c-MYC antibodies. **Scale bar** corresponds to 50 μm. **C)** Immunoblots using the stated antibodies of lysates from GRHL3-kd and Scr OKF-6 cells grown in serum, or transduced with pTRIPZ vector containing S9A GSK3B as indicated. HSP70 served as the loading control. Quantitation of expression relative to the Scr control and normalized to the loading control as measured by densitometry is shown under each lane. **D)** Growth curves of the cell lines listed in **(C)**. 5 X 10^3 cells for each line were seeded at day 0. The differences between cell numbers at day 8 were statistically significant ($P < .001$ Scr vs GRHL3-kd; $P = .003$ GRHL3-kd + GSK3B vs GRHL3-kd) using a two-sided Student's *t* test. The **error bars** represent the standard deviation (±SD).

ARTICLE

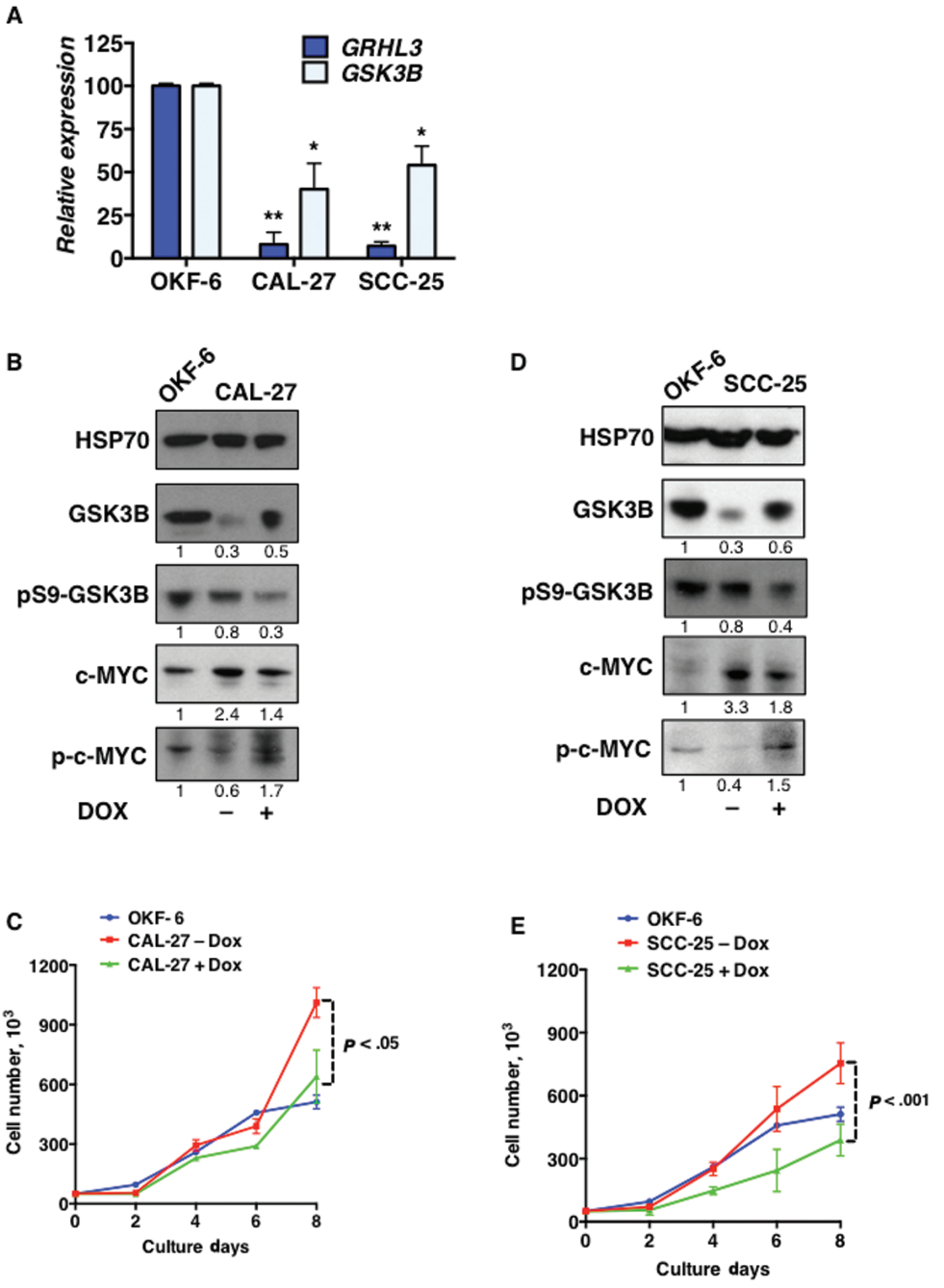

Figure 8. Effects of restoration of GSK3B expression on human head and neck squamous cell carcinoma (HNSCC) proliferation. **A)** Quantitative real-time polymerase chain reaction (qRT-PCR) of *GRHL3* and *GSK3B* expression in OKF-6, CAL-27, and SCC-25 cells. *HPRT* served as the control. The differences in expression of both genes between OKF6 and the HNSCC lines were statistically significant (*GRHL3* expression $P = .005$ OKF-6 vs CAL-27, $P = .001$ OKF-6 vs SCC-25; *GSK3B* expression $P = .045$ OKF-6 vs CAL27, $P = .03$ OKF-6 vs SCC-25) using a two-sided Student's *t* test. Mean of three independent experiments ± SD. **B)** Immunoblots using the stated antibodies of lysates from OKF-6 cells and CAL-27 cells transduced with the pTRIPZ vector containing an inducible FLAG-tagged S9A GSK3B and grown in the presence and absence of doxycycline for eight days, as indicated. HSP70 served as the loading control. Quantitation of expression relative to OKF-6 and normalized to the loading control as measured by densitometry is shown under each lane. **C)** Growth curves of the cell lines listed in **(B)**. 5 X 10^3 cells for each line were seeded at day 0. The differences between cell numbers at day 8 were statistically significant ($P = .04$) using two-sided Student's *t* test. The **error bars** represent the standard deviation (±SD). **D)** Immunoblots using the stated antibodies of lysates from OKF-6 cells and SCC-25 cells transduced with pTRIPZ vector containing an inducible FLAG-tagged S9A GSK3B and grown in the presence and absence of doxycycline for eight days, as indicated. HSP70 served as the loading control. Quantitation of expression relative to OKF-6 and normalized to the loading control as measured by densitometry is shown under each lane. **E)** Growth curves of the cell lines listed in **(B)**. 5 X 10^3 cells for each line were seeded at day 0. The differences between cell numbers at day 8 were statistically significant ($P < .001$) using two-sided Student's *t* test. The **error bars** represent the standard deviation (±SD).

and cell lines, we show that loss of *GRHL3* induces HNSCC through reduced expression of the direct target gene *GSK3B*. *GRHL3* and *GSK3B* are co-expressed in the oral epithelium (27,28) and exhibit reduced expression/inactivation in human HNSCC (29–31) that is associated with a poor prognosis (32,33). Mice deficient for either factor exhibit an increased propensity to HNSCC with exposure to the oral carcinogen 4-NQO.

Although *GSK3B* has been thought to be constitutively expressed and primarily regulated by site-specific phosphorylation of the S9 and Y216 residues (34,35), our findings alter

this paradigm in one setting, by establishing the pivotal importance of tissue-specific transcriptional control in suppression of HNSCC. Parallels exist with the GRHL3-dependent regulation of *PTEN* in the epidermis (8). Despite their common embryonic origins, the signaling pathways induced by loss of *Grhl3* in mice differed markedly between epidermis and oral epithelium. The characteristic reduction in PTEN with activation of PI3K/AKT/mTOR and complete loss of p-ERK expression seen in *Grhl3*-deficient skin SCC (8) was never observed in the HNSCC in these animals. Although recent data demonstrated that *Pten* deletion in oral epithelium in mice is a driver of HNSCC in the 4-NQO model (36), previous studies demonstrated that spontaneous HNSCC in these mice occurs infrequently (11). This suggests that in mice lacking *Grhl3* loss of GSK3B is a more potent stimulus for development of HNSCC than loss of PTEN. As a corollary, loss of GSK3B expression and stabilization of c-MYC was never observed in *Grhl3*-deficient skin SCC in mice or humans, and knockdown of GRHL3 in normal keratinocytes did not lead to reduced levels of GSK3B.

In human HNSCC, substantial heterogeneity is observed. All tumors display low levels of *GRHL3*, but in some, this is accompanied by a reduction in *GSK3B*, in others *PTEN*, and in a few expression of both targets is reduced. This heterogeneity may reflect additional mutations in some human HNSCC that favor activation of the PI3K/AKT/mTOR pathway over GSK3B/c-MYC. An obvious candidate here is PTEN itself, which is mutated in 5% to 23% of human HNSCC (2,10,26,37). Cell lines derived from human HNSCC reflect this variation, with SCC-25 cells showing reduced growth kinetics with restoration of GSK3B and reduced c-MYC expression, but SCC-9 cells were responsive to enhanced PTEN expression, with suppression of PI3K/AKT/mTOR signalling (8). Deciphering which of these pathways is active in an individual tumor may prove instructive as to the most effective therapy. One constant in all the tumors we examined was the reduction in *GRHL3* expression, suggesting that this factor may be central in the pathogenesis of many HNSCCs. Supporting this are recent reports of altered expression of several key regulators of *GRHL3* in HNSCC. miR-21, which we have previously shown to be a critical suppressor of *GRHL3* expression (8), has been shown in multiple studies to be upregulated in HNSCC (38–40) and to confer a poor prognosis (41). *IRF6* and *TP63*, which have both recently been implicated as drivers of HNSCC (2), are known transcriptional regulators of *Grhl3* (42,43), as is *TP53* (44), which is mutated in 47% of HNSCCs (37).

c-MYC lies downstream of GRHL3/GSK3B in the promotion of HNSCC in both mice and humans. The upregulation of c-MYC in the embryonic tongue epithelium from *Grhl3*-null mice, and in the spontaneous tumors in aged *Grhl3*-deficient mice (not shown), is indicative of a cell-autonomous effect because of loss of GRHL3/GSK3B, rather than a secondary effect of 4-NQO exposure. Consistent with this, K5 *Myc* transgenic mice develop spontaneous tumors that predominantly affect the oral epithelium (45). Elevated expression of *c-MYC* is evident in human HNSCC and is associated with a poor prognosis (46–50). Multiple mechanisms underpin the deregulated expression of *c-MYC* in tumor cells, including gene amplification, chromosomal translocations, single nucleotide polymorphisms in regulatory regions, and enhanced stability of the protein (51,52). This latter mechanism may explain discrepancies observed between *c-MYC* gene amplification or mRNA expression and high levels of c-MYC protein in many tumors (53). The stability of c-MYC protein is regulated by phosphorylation at conserved residues, S62 and T58 (24). Increased c-MYC stability occurs in response to ERK signalling with phosphorylation at S62, whereas subsequent phosphorylation at T58 by GSK3B leads to ubiquitination by the SCF-Fbw7 E3 ligase and proteosomal degradation (23,54). The combination of sustained p-ERK expression (unlike in skin SCC) and loss of GSK3B observed in the HNSCC in mice provides the ideal combination for enhanced c-MYC stability, which has been linked to potentiation of tumorigenic activity (55,56).

One limitation of our study is that loss of GRHL3 in human HNSCC is induced through overexpression of miR-21 (8–10), whereas in mice this is achieved by genetic deletion. This may account for the heterogeneity of dysregulated signaling in human cancers, involving PTEN/PI3K/AKT and GSK3B/c-MYC, as opposed to the uniformity of defects in HNSCC in mice that are all centered on GSK3B/c-MYC. This uniformity also provides some limitations on using this mouse model to assess treatment strategies in HNSCC, and we are exploring miR-21–targeted approaches to circumvent this.

Nevertheless, our work provides a clear rationale for the use of targeted therapies in HNSCC based on the molecular signatures we have identified. Treatments with miR-21 antagonists may be effective in tumors lacking GRHL3 and, if combined with agents directed against either PI3K/AKT signalling or c-MYC, could target multiple drivers of the proto-oncogenic pathways. Inhibitors of PI3K/AKT signaling are already under investigation in HNSCC (1,57,58), and recent reports of pharmacological targeting of MYC using BET bromodomain inhibitors (59,60) may provide potentially novel therapeutic strategies for HNSCC.

Funding

This work was supported by grants from the Australian National Health and Medical Research Council (1049870 to SMJ) and the Association for International Cancer Research (to SMJ and CD).

Notes

We thank: Drs Rick Pearson and David Curtis for thoughtful comments on the manuscript; the Australian Phenomics Network Histopathology and Organ Pathology Service, University of Melbourne for analysis of tumors in the mice; the staff from the Bio21 Institute and ARL, Monash University for animal care; and the Victorian Cancer Biobank for human squamous cell carcinoma samples.

References

1. Leemans CR, Braakhuis BJ, Brakenhoff RH. The molecular biology of head and neck cancer. *Nat Rev Cancer*. 2011;11(1):9–22.
2. Stransky N, Egloff AM, Tward AD, et al. The mutational landscape of head and neck squamous cell carcinoma. *Science*. 2011;333(6046):1157–1160.
3. Jane SM, Ting SB, Cunningham JM. Epidermal impermeable barriers in mouse and fly. *Curr Opin Genet Dev*. 2005;15(4):447–453.
4. Venkatesan K, McManus HR, Mello CC, Smith TF, Hansen U. Functional conservation between members of an ancient duplicated transcription factor family, LSF/Grainyhead. *Nucl Acids Res*. 2003;31(15):4304–4316.
5. Wilanowski T, Tuckfield AM, Cerruti L, et al. A highly conserved novel family of mammalian developmental transcription factors related to Drosophila grainyhead. *Mech Dev*. 2002;114(1–2):37–50.
6. Ting SB, Caddy J, Hislop N, et al. A homolog of Drosophila grainy head is essential for epidermal integrity in mice. *Science*. 2005;308(5720):411–413.
7. Yu Z,Lin KK, Bhandari A, et al. The Grainyhead-like epithelial transactivator Get-1/Grhl3 regulates epidermal terminal differentiation and interacts functionally with LMO4. *Dev Biol*. 2006;299(1):122–136.
8. Darido C, Georgy SR, Wilanowski T, et al. Targeting of the tumor suppressor GRHL3 by a miR-21-dependent proto-oncogenic network results in PTEN loss and tumorigenesis. *Cancer Cell*. 2011;20(5):635–648.
9. Okami K, Wu L, Riggins G, et al. Analysis of PTEN/MMAC1 alterations in aerodigestive tract tumors. *Cancer Res*. 1998;58(3):509–511.
10. Poetsch M, Lorenz G, Kleist B. Detection of new PTEN/MMAC1 mutations in head and neck squamous cell carcinomas with loss of chromosome 10. *Cancer Genet Cytogenet*. 2002;132(1):20–24.

ARTICLE

11. Bian Y, Hall B, Sun ZJ, et al. Loss of TGF-beta signaling and PTEN promotes head and neck squamous cell carcinoma through cellular senescence evasion and cancer-related inflammation. *Oncogene*. 2012;31(28):3322–3332.
12. Suzuki A, Itamia S, Ohishi M, et al. Keratinocyte-specific Pten deficiency results in epidermal hyperplasia, accelerated hair follicle morphogenesis and tumor formation. *Cancer Res*. 2003;63(3):674–681.
13. Ting SB, Wilanowski T, Auden A, et al. Inositol- and folate-resistant neural tube defects in mice lacking the epithelial-specific factor Grhl-3. *Nature Med*. 2003;9(12):1513–1519.
14. Czerninski R, Amornphimoltham P, Patel V, Molinolo AA, Gutkind JS. Targeting mammalian target of rapamycin by rapamycin prevents tumor progression in an oral-specific chemical carcinogenesis model. *Cancer Prev Res*. 2009;2(1):27–36.
15. Tang XH, Knudsen B, Bemis D, Tickoo S, Gudas LJ. Oral cavity and esophageal carcinogenesis modeled in carcinogen-treated mice. *Clin Cancer Res*. 2004;10(1):301–313.
16. Stambolic V, Woodgett JR. Mitogen inactivation of glycogen synthase kinase-3 beta in intact cells via serine 9 phosphorylation. *Biochem J*. 1994;303 (3):701–704.
17. Fuchs E, Raghavan S. Getting under the skin of epidermal morphogenesis. *Nature Rev Genet*. 2002;3(3):199–209.
18. Ouhayoun JP, Gosselin F, Forest N, Winter S, Franke WW. Cytokeratin patterns of human oral epithelia: differences in cytokeratin synthesis in gingival epithelium and the adjacent alveolar mucosa. *Differentiation*. 1985;30(2): 123–129.
19. Caddy J, Wilanowski T, Darido C, et al. Epidermal wound repair is regulated by the planar cell polarity signaling pathway. *Dev Cell*. 2010;19(1):138–147.
20. Ma C, Wang J, Gao Y, et al. The role of glycogen synthase kinase 3beta in the transformation of epidermal cells. *Cancer Res*. 2007;67(16):7756–7764.
21. Mishra R. Glycogen synthase kinase 3 beta: can it be a target for oral cancer. *Mol Cancer*. 2010;9:144.
22. Eversole LR, Sapp JP. c-myc oncoprotein expression in oral precancerous and early cancerous lesions. *Eur J Cancer*. 1993;29B(2):131–135.
23. Gregory MA, Qi Y, Hann SR. Phosphorylation by glycogen synthase kinase-3 controls c-myc proteolysis and subnuclear localization. *J Biol Chem*. 2003;278(51):51606–51612.
24. Sears RC. The life cycle of C-myc: from synthesis to degradation. *Cell Cycle*. 2004;3(9):1133–1137.
25. Murphy DJ, Junttila MR, Pouyet L, et al. Distinct thresholds govern Myc's biological output in vivo. *Cancer Cell*. 2008;14(6):447–457.
26. Shao X, Tandon R, Samara G, et al. Mutational analysis of the PTEN gene in head and neck squamous cell carcinoma. *Int J Cancer*. 1998;77(5): 684–688.
27. Auden A, Caddy J, Wilanowski T, Ting SB, Cunningham JM, Jane SM. Spatial and temporal expression of the Grainyhead-like transcription factor family during murine development. *Gene Expr Patterns*. 2006;6(8): 964–970.
28. He F, Popkie AP, Xiong W, et al. Gsk3beta is required in the epithelium for palatal elevation in mice. *Dev Dyn*. 2010;239(12):3235–3246.
29. Amornphimoltham P, Sriuranpong V, Patel V, et al. Persistent activation of the Akt pathway in head and neck squamous cell carcinoma: a potential target for UCN-01. *Clin Cancer Res*. 2004;10(12):4029–4037.
30. Chun KH, Lee HY, Hassan K, Khuri F, Hong WK, Lotan R. Implication of protein kinase B/Akt and Bcl-2/Bcl-XL suppression by the farnesyl transferase inhibitor SCH66336 in apoptosis induction in squamous carcinoma cells. *Cancer Res*. 2003;63(16):4796–4800.
31. Kang T, Wei Y, Honaker Y, et al. GSK-3 beta targets Cdc25A for ubiquitin-mediated proteolysis, and GSK-3 beta inactivation correlates with Cdc25A overproduction in human cancers. *Cancer Cell*. 2008;13(1):36–47.
32. Goto H, Kawano K, Kobayashi I, Sakai H, Yanagisawa S. Expression of cyclin D1 and GSK-3beta and their predictive value of prognosis in squamous cell carcinomas of the tongue. *Oral Oncol*. 2002;38(6):549–556.
33. Rickman DS, Millon R, De Reynies A, et al. Prediction of future metastasis and molecular characterization of head and neck squamous-cell carcinoma based on transcriptome and genome analysis by microarrays. *Oncogene*. 2008;27(51):6607–6622.
34. Doble BW Woodgett JR. GSK-3: tricks of the trade for a multi-tasking kinase. *J Cell Sci*. 2003;116(Pt 7):1175–1186.
35. Sutherland C, Leighton IA, Cohen P. Inactivation of glycogen synthase kinase-3 beta by phosphorylation: new kinase connections in insulin and growth-factor signalling. *Biochem J*. 1993;296 (Pt 1):15–19.
36. Squarize CH, Castilho RM, Abrahao AC, Molinolo A, Lingen MW, Gutkind JS. PTEN deficiency contributes to the development and progression of head and neck cancer. *Neoplasia*. 2013;15(5):461–471.
37. Agrawal N, Frederick MJ, Pickering CR, et al. Exome sequencing of head and neck squamous cell carcinoma reveals inactivating mutations in NOTCH1. *Science*. 2011;333(6046):1154–1157.
38. Volinia S, Calin GA, Liu CG, et al. A microRNA expression signature of human solid tumors defines cancer gene targets. *Proc Natl Acad Sci U S A*. 2006;103(7):2257–2261.
39. Avissar M, McClean MD, Kelsey KT, Marsit CJ. MicroRNA expression in head and neck cancer associates with alcohol consumption and survival. *Carcinogenesis*. 2009;30(12):2059–2063.
40. Hui AB, Lenarduzzi M, Krushel T, et al. Comprehensive MicroRNA profiling for head and neck squamous cell carcinomas. *Clini Cancer Res*. 2010;16(4):1129–1139.
41. Fu X, Han Y, Wu Y, et al. Prognostic role of microRNA-21 in various carcinomas: a systematic review and meta-analysis. *Eur J Clin Invest*. 2011;41(11):1245–1253.
42. de la Garza G, Schleiffarth JR, Dunnwald M, et al. Interferon regulatory factor 6 promotes differentiation of the periderm by activating expression of Grainyhead-like 3. *J Invest Dermatol*. 2013;133(1):68–77.
43. Zarnegar BJ, Webster DE, Lopez-Pajares V, et al. Genomic profiling of a human organotypic model of AEC syndrome reveals ZNF750 as an essential downstream target of mutant TP63. *Am J Hum Genet*. 2012;91(3):435–443.
44. Brynczka C, Labhart P, Merrick BA. NGF-mediated transcriptional targets of p53 in PC12 neuronal differentiation. *BMC Genomics*. 2007;8:139.
45. Rounbehler RJ, Schneider-Broussard R, Conti CJ, Johnson DG. Myc lacks E2F1's ability to suppress skin carcinogenesis. *Oncogene*. 2001;20(38):5341–5349.
46. Pelengaris S, Khan M, Evan G. c-MYC: more than just a matter of life and death. *Nature Rev Cancer*. 2002;2(10):764–776.
47. Akervall J, Bockmuhl U, Petersen I, Yang K, Carey TE, Kurnit DM. The gene ratios c-MYC:cyclin-dependent kinase (CDK)N2A and CCND1:CDKN2A correlate with poor prognosis in squamous cell carcinoma of the head and neck. *Clin Cancer Res*. 2003;9(5):1750–1755.
48. Field JK, Spandidos DA, Stell PM, Vaughan ED, Evans GI, Moore JP. Elevated expression of the c-myc oncoprotein correlates with poor prognosis in head and neck squamous cell carcinoma. *Oncogene*. 1989; 4(12):1463–1468.
49. Perez-Sayans M, Suarez-Penaranda JM, Pilar GD, Barros-Angueira F, Gandara-Rey JM, Garcia-Garcia A. What real influence does the proto-oncogene c-myc have in OSCC behavior? *Oral Oncol*. 2011;47(8):688–692.
50. Rodrigo JP, Lazo PS, Ramos S, Alvarez I, Suarez C. MYC amplification in squamous cell carcinomas of the head and neck. *Arch Otolaryngol*. 1996;122(5):504–507.
51. Meyer N, Penn LZ. Reflecting on 25 years with MYC. *Nature Rev Cancer*. 2008;8(12):976–990.
52. Eilers M, Eisenman RN. Myc's broad reach. *Genes Dev*. 2008;22(20):2755–2766.
53. Junttila MR, Westermarck J. Mechanisms of MYC stabilization in human malignancies. *Cell Cycle*. 2008;7(5):592–596.
54. Welcker M, Orian A, Jin J, et al. The Fbw7 tumor suppressor regulates glycogen synthase kinase 3 phosphorylation-dependent c-Myc protein degradation. *Proc Natl Acad Sci U S A*. 2004;101(24):9085–9090.
55. Wang X, Cunningham M, Zhang X, et al. Phosphorylation regulates c-Myc's oncogenic activity in the mammary gland. *Cancer Res*. 2011;71(3):925–936.
56. Yeh E, Cunningham M, Arnold H, et al. A signalling pathway controlling c-Myc degradation that impacts oncogenic transformation of human cells. *Nature Cell Biol*. 2004;6(4):308–318.
57. Wang Z, Martin D, Molinolo AA, et al. mTOR co-targeting in cetuximab resistance in head and neck cancers harboring PIK3CA and RAS mutations. *J Natl Cancer Inst*. 2014;106(9):dju215 doi:10.1093/jnci/dju215.
58. D'Amato V, Rosa R, D'Amato C, et al. The dual PI3K/mTOR inhibitor PKI-587 enhances sensitivity to cetuximab in EGFR-resistant human head and neck cancer models. *Br J Cancer*. 2014;110(12):2887–2895.
59. Delmore JE, Issa GC, Lemieux ME, et al. BET bromodomain inhibition as a therapeutic strategy to target c-Myc. *Cell*. 2011;146(6):904–917.
60. King B, Trimarchi T, Reavie L, et al. The ubiquitin ligase FBXW7 modulates leukemia-initiating cell activity by regulating MYC stability. *Cell*. 2013;153(7):1552–1566.